RSC Advances

PAPER

View Article Online
View Journal | View Issue

Cite this: *RSC Adv.*, 2015, **5**, 60993

Facile surface tailoring of metal oxide nanoparticles *via* a two-step modification approach†

A. Kockmann, J. Hesselbach, S. Zellmer, A. Kwade and G. Garnweitner*

Received 13th May 2015
Accepted 6th July 2015

DOI: 10.1039/c5ra08932h

www.rsc.org/advances

The tailoring of surface properties of metal oxide nanoparticles is highly important to exploit their benefits in an optimal way for diverse applications. For example, in polymer matrix nanocomposites one of the most critical aspects is the interaction of the particles with the matrix, which is determined by the chemistry of the particle surface and can be adjusted by attachment of organic ligands. Whilst many empirical solutions have been presented for specific combinations of particles and matrix, generalized approaches are not available yet. As a versatile and arbitrary method to permanently modify the surface of metal oxide nanoparticles, we present a two-step approach and prove its applicability for the versatile adjustment of surface properties of two types of nanoparticles.

Introduction

Owing to their simple processing, low cost, and good availability, polymer composites and thin films have become more and more widely used over the last decades.[1–3] To further improve their properties or introduce novel functional properties, the addition of nanoscale filler particles is intensively investigated to achieve highly homogeneous nanocomposites. Due to their high thermal and chemical stability and good availability, metal oxide nanoparticles (NPs) have become a major class of functional particulate fillers in polymeric nanocomposites, aiming at a broad spectrum of applications *e.g.* from lightweight structures for aircrafts,[4,5] thermally conductive and electrically insulating layers for electric circuits,[6–8] transparent composites[9–13] to dielectric coatings with high permittivity.[14–16] In the last decades, great efforts were made to achieve the controlled synthesis of metal oxide NPs.[17–28] Although many examples for the successful application of metal oxide NPs in nanocomposites were reported,[1,18,29–36] their efficacy often is limited, since the chemical structure of the particle surface is determined by the utilized synthesis. Typically, surface bound organic groups from the precursor and solvent affect the interaction between the resin and solvent with the particle surface. In the case of a pyrolytic synthesis, most of the organics are decomposed due the high reaction temperature, but these methods greatly suffer from the consequent formation of stable secondary structures like aggregates.[20,37–39] Small colloidally stable particles (with a narrow size distribution) are needed to achieve the desired properties of nanocomposites.[40] The use of specialized organic stabilizers or capping agents added *in situ* during the synthesis or alternatively afterwards in a wet chemical process can lead to stable dispersions of nanoparticles, but frequently the created effect is limited and the ligand can be removed easily from the particle surface. Furthermore, for many applications that aim at enhanced mechanical performance, a covalent binding between the NPs and the surrounding matrix is desired for optimum properties. Grafting-from and grafting-to approaches were developed to generate polymer shells which are strongly bound to the particle surface.[1,41,42] These strategies involve the coupling of a polymer chain or alternatively of polymer precursors or initiators with the particles, followed by subsequent polymerisation. In these approaches ligands have to be designed which needs to be synthesised, purified and tested for a successful binding with the particle surface as well as polymerization reaction. Also in cases where a molecular ligand is used to improve the compatibility between nanoparticle filler and the surrounding matrix without covalent linkage, a specific ligand must be identified which implies an extensive optimization before the desired performance is achieved. In this work, we present a two-step approach to achieve the covalent attachment of a large variety of organic groups with specific functionality to the surface of metal oxide NPs. In our process a standard multifunctional ligand is covalently attached to the particles in the first step and subsequently coupled with different organic species *via* a standard organic condensation reaction in the second step, which we prove to be achieved for different nanoparticle systems. For this purpose, in the first step we investigated the modification of different metal oxide NPs (both commercial NPs from pyrolysis and custom-made NPs from a non-aqueous synthesis) with 3-aminopropyltriethoxysilane (APTES), to achieve the covalent attachment of chemically available amino groups to the particle surface, which

Institute for Particle Technology, Technische Universität Braunschweig, 38104 Braunschweig, Germany. E-mail: g.garnweitner@tu-bs.de

† Electronic supplementary information (ESI) available: Elemental analysis of modified silica nanoparticles; particle size distribution of ZrO_2 nanoparticles after 2-step modification; TEM images and FT-IR spectra of modified ZrO_2 and Al_2O_3 nanoparticles. See DOI: 10.1039/c5ra08932h

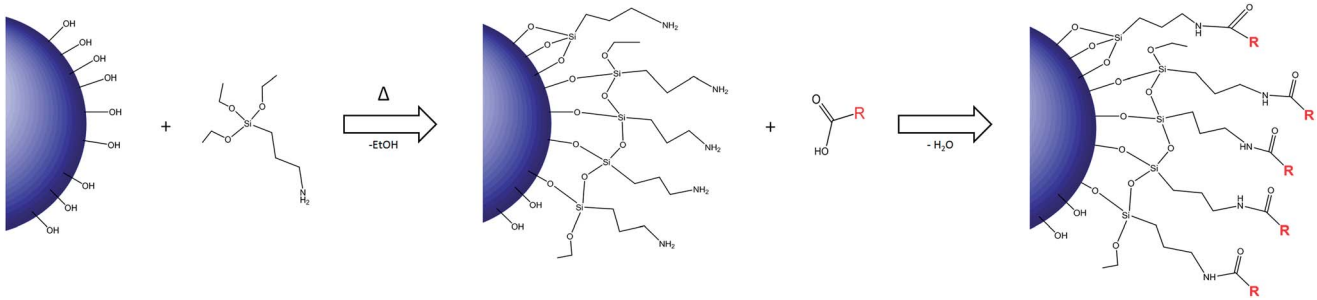

Fig. 1 Scheme of the two-step modification strategy.

is proven by chemical and elemental analyses. In the second step, an organic coupling mechanism in analogy to the Merrifield synthesis[43] is used to achieve the formation of amide bonds between the amino group and different carboxylic acids. The reaction scheme is shown in Fig. 1. The type and specification of the coupled carboxylic acid is then shown to define the chemical properties of the nanoparticles after the modification procedure.

Experimental

2.1 Synthesis of nanoparticles

The used zirconia (ZrO_2) nanoparticles were synthesized by the non-aqueous sol–gel synthesis as we described earlier.[12] 80 mL of Zr(IV)*n*-propoxide in 1-propanol (70 wt%, Aldrich) was added to 920 mL of benzyl alcohol as reaction medium and reacted for 24 h at 250 °C in a steel reactor (Polyclave type 3/1, Büchi Glas Uster, external thermostat: Huber Tango HT). After the reaction, a suspension of 3 nm-sized ZrO_2 particles with a solid content of 22 g L^{-1} was obtained. Alumina (γ-Al_2O_3) particles were purchased as dry powder from Evonik Industries (AluC©) and dispersed for 2 hours with a laboratory scale planetary ball mill (Retsch PM400, 250 rpm) in ethanol. In this process, a filling ratio of the grinding media of 30 vol% was used. As grinding media, yttrium stabilized zirconium oxide beads (SiLibeads, Sigmund Lindner GmbH) with a mean diameter of 0.2 mm were inserted to obtain an appropriate alumina particle size of 100 nm with a solid content of 78 g L^{-1}. Furthermore, silica (SiO_2) nanoparticles with a particle size of 160 nm were synthesized by a Stöber process (see ESI† for details).

2.2 Nanoparticle surface modification

For the first surface modification step – the coupling of (3-aminopropyl)triethoxysilane (APTES, 99%, Aldrich) – the particle suspensions were sonicated for 1 h in an ultrasonic bath to disperse the zirconia agglomerates and to ensure fine dispersed the alumina particles, respectively. Afterwards, the suspensions were filled into round bottom flasks and a standard amount of 1 mol APTES/mol ZrO_2 or Al_2O_3 was added and heated into reflux for 12 h (for benzyl alcohol, 130 °C was used). To induce precipitation of the APTES-modified particles in solution, hexane (tech.) was added with a volume ratio of 1 : 1 (hexane : particle dispersion). After centrifugation at 7500 rpm for 15 minutes, the particles were redispersed in ethanol and again precipitated with hexane. This washing procedure was repeated three times to remove unreacted APTES. Finally, the APTES-modified particles were dried at room temperature under vacuum.

In the second step – the coupling of carboxylic acids – the APTES-modified particles were dispersed in ethanol (10 wt%) using magnetic stirring for 30 minutes and then added to a saturated solution of the respective carboxylic acid and *N*,*N*′-diisopropylcarbodiimide (DIC, molar ratio 1 : 1.5) as an activator for the carboxyl group in ethanol (named as APTES-CA-

Table 1 Specifications of the used carboxylic acids

Carboxylic acid	Purity	Company	Type (number of carbon atoms)
Malonic acid	>98%	Fluka	Dicarboxylic acid (3)
Sorbic acid	>99%	Aldrich	Unsaturated (6)
Hexanoic acid	99.5%	Aldrich	Saturated (6)
Adipic acid	99.5%	Aldrich	Dicarboxylic acid (3)
Benzoic acid	99%	Riedel-de Haen	Unsaturated, aromatic (7)
Heptanoic acid	96%	Aldrich	Saturated (7)
Octanoic acid	99%	Aldrich	Saturated (8)
Perfluorooctanoic acid	96%	Aldrich	Saturated (8)
Undecylenic acid	95%	Aldrich	Unsaturated (11)
Undecanoic acid	98%	Fluka	Saturated (11)
Stearic acid	95%	Aldrich	Saturated (18)

modified particles). The coupling reactions were carried out for 10 h. The APTES-CA-modified particles were precipitated by adding either hexane or deionized water, depending on the used carboxylic acid, and subsequently redispersed and washed three times with an adequate mixture of either ethanol/hexane or ethanol/water to remove all side products. Table 1 shows the utilized carboxylic acids.

After the two-step modification, NP-based coatings were fabricated *via* drop-casting of the suspensions with 10 wt% of modified particles in ethanol onto a glass substrate (IDL, 76 × 26 mm) were dried afterwards for 2 h at room temperature and subsequently for 5 h at 100 °C.

2.3 Characterization

Powder X-ray diffraction (PXRD) (Cu K_α radiation; Empyrean Cu LEF HR goniometer; Empyrean series 2, PANalytical; PIXcel-3D detector) was utilized to determine the phase and crystallinity of the particles. The primary particle size of the zirconia NPs was determined using the Scherrer equation. The ninhydrin tests (Kaiser tests) were performed using a 1 wt% solution of ninhydrin in ethanol, which was added to a 10 wt% particle suspension (or the supernatant without particles) in ethanol and heated to 60 °C for 20 minutes. For a positive result, the solutions (with or without particles) assume dark blue color. Dynamic light scattering (DLS; Nanophox, Sympatec GmbH) was executed using diluted samples in ethanol to determine the secondary particle sizes and particle size distributions. The quantity of C, H and N of the particle surface after modification was determined by elemental analysis using a FlashEA 1112. TEM images of the synthesised particles were made with a LEO 922 A from Carl Zeiss at 200 kV and can be found in the ESI section (Fig. S3†). FT-IR spectra (see ESI, Fig. S5–S7†) were measured on an ATR Tensor 27 by Bruker. To generate SEM images of the coatings an EVO scanning electron microscope (Zeiss) coupled with energy-dispersive X-ray spectroscopy (EDX, Bruker) was used. The contact angle measurements were performed on a Drop Shape Analysis DAS 100 device (Krüss) in conformity with the DIN EN 828:2013-04 standard, whereby 6 μL deionized water was dosed with a pump speed of 100 μL min^{-1} and deposited on the samples. For each coating, five drops were measured three times each.

Results and discussion

3.1 Nanoparticle modification

First step: APTES modification. After the synthesis and preparation of the different particle dispersions, the first modification step with APTES was realized. In order to investigate the adsorption of APTES on the NP surface for the two systems, a reaction mixture of each system (10 wt%) with an APTES : particle weight ratio of 0.2 was prepared and reacted for 48 h. The content of surface bound APTES was measured by elemental analysis of the dried powders withdrawn after different reaction times (30 min, 1 h, 3 h, 6 h, 10 h, 48 h). In Fig. 2 the carbon and nitrogen contents of APTES-modified alumina NPs are shown for different reaction times. An increase of the reaction time leads to a higher amount of APTES adsorbed to the particle surface and thus to higher carbon and nitrogen contents. After around 10 h of reaction almost the full amount of the added APTES is bound and a monomolecular reaction (pseudo-first order) can be assumed with the APTES as the reactant with limited availability. This is confirmed by the fact that higher quantities of APTES can bind to the alumina NPs as shown in Fig. 3 (top).

Different ratios of APTES/NPs were investigated, whereby the volume and concentration of the NP dispersions (alumina (top), zirconia (bottom)) were kept constant and the amount of added APTES was varied. It is shown that for a small APTES/NP ratio the carbon and nitrogen contents of the modified NPs increase nearly linearly with the used APTES content, so that the coordination of all added APTES can be assumed. For higher APTES/NP ratios the slope decreases and a plateau is reached, which indicates a hindered reaction of further APTES, *i.e.* the surface becomes fully covered with the silane and no coupling exceeding monomolecular coverage occurs. Furthermore, the content of APTES bound to the particle surface strongly influences the secondary particle size, since the amino groups also lead to a stabilising effect in polar solvents. Unmodified zirconia particles are organophilic right after the synthesis and could not be stabilized in polar solvents like ethanol. With an increasing amount of APTES on the NP surface, the secondary particle size (measured by DLS) sharply decreases from around 200 nm at 10 wt% APTES/ZrO_2 ratio to 3.2 nm for NP with an APTES-saturated surface, which is in accordance with the crystallite size of these NPs of around 3–3.5 nm (measured with PXRD, calculated using the Scherrer equation).[15] Fig. 4 illustrates that an increase of the content of bound APTES from 10 to 30 wt% leads to a stabilization of the NPs to the primary particle size level. For very high APTES contents such as 125 wt%, an even smaller secondary size with a broader particle size distribution can be determined by DLS: this can be attributed to the weak signal intensity. In conclusion, the successful coordination of APTES to the surface of alumina and ZrO_2 NPs can be shown, with the binding of APTES not only leading to increased carbon and nitrogen contents, but also to stabilization of the

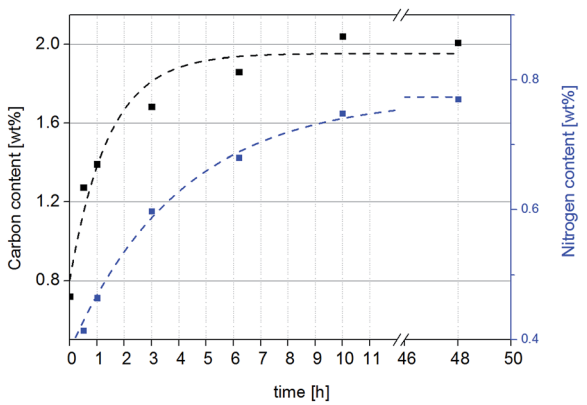

Fig. 2 Carbon and nitrogen contents of APTES-modified alumina particles at different times of reaction with APTES (APTES/Al_2O_3 wt ratio 1 : 5).

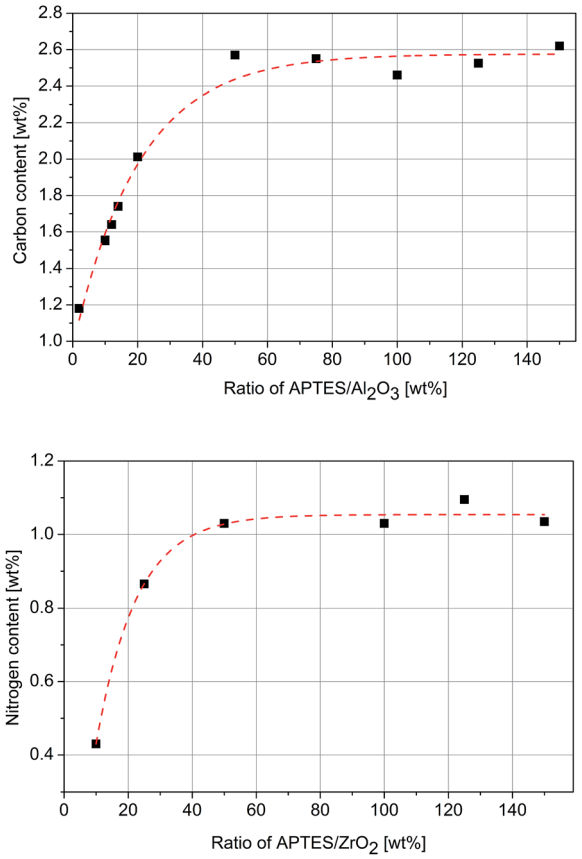

Fig. 3 Carbon content of APTES modified alumina particles with different APTES/Al_2O_3 ratios after 24 h of reaction (top) and nitrogen content of APTES-modified zirconia particles with different APTES/ZrO_2 ratios after 24 h of reaction (bottom).

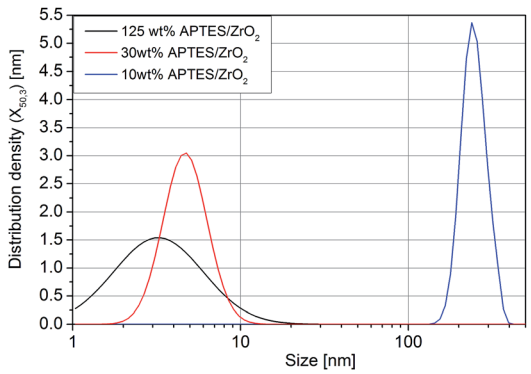

Fig. 4 Particle size distributions of zirconia nanoparticles after modification with different contents of APTES/particle as measured by DLS.

NPs down to the primary particle size for optimum APTES amounts. Analogously, also the modification of SiO_2 nanoparticles obtained by Stöber synthesis is possible (see Fig. S1, ESI†).

In addition to the successful modification, the presence of available and reactive amino groups was proven by the ninhydrin test. In Fig. 5, a typical result of a ninhydrin test of a dispersion of APTES-modified NPs (alumina) is shown (left). The available and reactive amino groups at the particle surface after the first modification step react with the ninhydrin reagents and the NP assume a dark blue color. It is noteworthy that the ninhydrin test of the particle supernatant after the first modification step is negative (not shown), hence it can be concluded that APTES is either firmly bound or fully removed from the NPs by washing.

Second step: reaction with carboxylic acids. The APTES-modified NPs can be directly used as stable and reactive filler particles to be embedded in epoxy-based resins. However, for a versatile surface chemistry the attachment of different types of organic functions ranging from polymerizable groups to superhydrophobic fluorinated alkane chains is desired. To this end, the further modification of the APTES-modified NPs *via* the coupling of carboxylic acids with a broad variety of chemical functions was performed. To show the covalent coupling of the added carboxylic acids to the amino-terminated APTES-NPs in the second modification step, ninhydrin tests before and after the second step were carried out, showing a negative result after the coupling step (Fig. 5). The secondary particle size also increases significantly after the coupling of non-polar carboxylic acids due to agglomeration of the NPs in the polar solvent (see Fig. S4, ESI†). Furthermore, an increase of the carbon content of the modified NPs (measured after several washing steps) can be associated with the successful amide formation. To investigate the influence of the chain length and the functionality of different carboxylic acids on the surface chemistry, alumina and zirconia particles were modified with a variety of different carboxylic acids. Fig. 6 (top) shows the carbon and hydrogen contents of two-step-modified alumina NPs for different carboxylic acids used in the second modification step.

A straightforward correlation between the used carboxylic acid and the observed carbon and hydrogen contents of the functionalized NPs is visible. NPs after modification with longer-chain carboxylic acids, such as stearic acid, undecylenic or undecanoic acid show significantly higher carbon and hydrogen contents than NPs modified with acids of shorter chain length; thereby APTES-modified alumina particles are shown as reference. The type of carboxylic acid used (saturated, unsaturated or substituted) is further reflected in the hydrogen content as compared to the carbon content, whereby the values

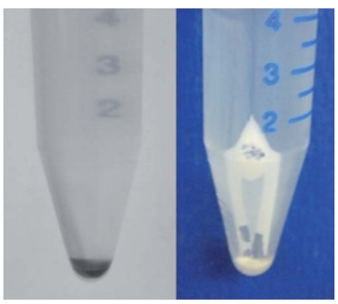

Fig. 5 Photographs of ninhydrin tests performed on suspensions of APTES modified NPs (left, positive) and APTES-CA modified NPs (right, negative).

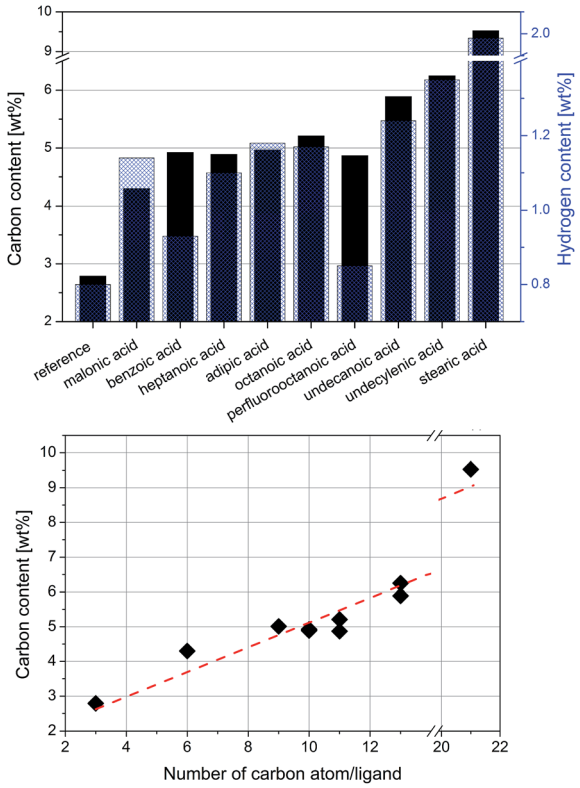

Fig. 6 Carbon (black, solid) and hydrogen (blue, dotted) contents at the surface of alumina NPs after two-step modification with different carboxylic acids (top) and carbon contents of alumina NPs modified with different carboxylic acids as a function of their chain length (bottom).

for unsaturated acids, such as benzoic acid and undecylenic acid, are clearly smaller than for saturated acids and again smaller than for dicarboxylic acids (malonic and adipic acid). Fig. 6 (bottom) shows the correlation between the carbon content of modified NPs after the second modification step and the number of carbon atoms of the respective carboxylic acid. For NPs modified with perfluorooctanoic acid, the hydrogen as well as the carbon content is lower than for octanoic acid, which was expected because of the substitution of the hydrogen atoms by the much heavier fluorine atoms.

In the case of the zirconia particles, carboxylic acids with an equal chain length of six carbon atoms but different functionalities were used as well as perfluorooctanoic acid (Fig. 7). As expected for an equal carbon chain length, similar carbon contents for all samples were measured except for PFOA where again a lower content arises from substitution. In comparison to the alumina particle system, higher absolute values were detected due to the smaller particle size and, thus, a larger specific surface area of the nanoparticles.

By comparing the hydrogen and carbon contents, the type of used carboxylic acid can be determined. Again, NPs modified with unsaturated acids show significantly lower hydrogen contents than particles that are modified with saturated or even bifunctional carboxylic acids. The higher hydrogen/carbon ratio of the adipic acid-modified NPs compared to hexanoic acid is explained by the fact that due to the polar (carboxyl) groups a

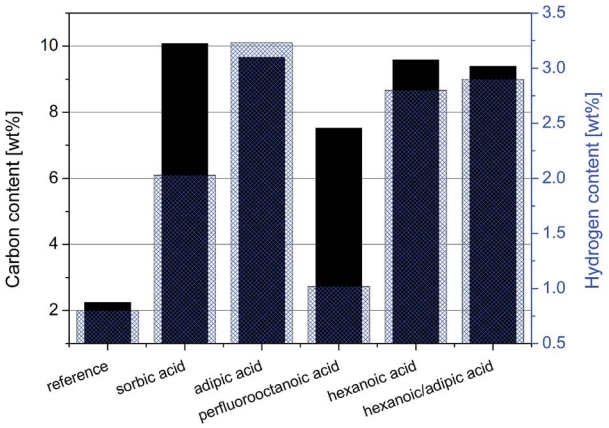

Fig. 7 Carbon (black, solid) and hydrogen (blue, dotted) contents of zirconia NPs after two-step modification with different carboxylic acids.

significant amount of water (air moisture) is adsorbed to the particles after drying and exposure to ambient conditions. To show that this approach is versatile, silica particle were treated in an analogous manner. Elemental analysis of silica particles after coupling of different carboxylic acids (see Fig. S2, ESI†) shows comparable results, proving the successful modification.

Furthermore, the covalent coupling of the carboxylic acids is evidenced by FT-IR spectroscopy. FT-IR spectra of the NPs after the second modification step (Fig. S5–S7, ESI†) show typical absorption bands corresponding to the utilized acid chain as well as new double peaks for the established peptide bond, which proves the expected covalent binding.

3.2 Characterization of NP properties

For the application in easy-to-clean surface coatings, perfluorooctanoic acid was used to generate highly hydrophobic particle surfaces. For a further characterization of the

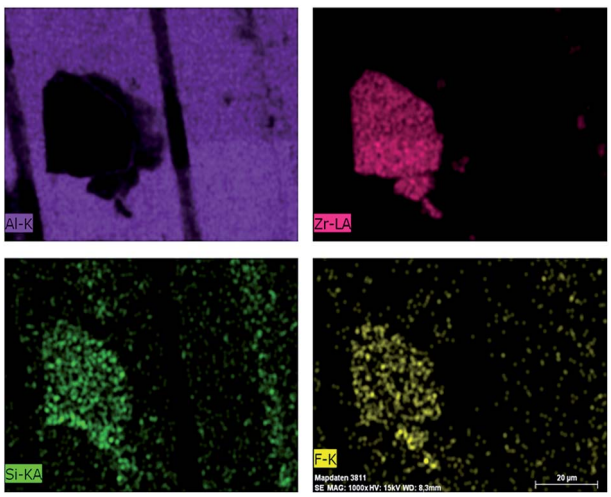

Fig. 8 Aluminum (purple), zirconium (pink), silicon (red) and fluorine (yellow) contents of zirconia particles modified with APTES (first step) and perfluorooctanoic acid (second step).

perfluorooctanoic acid modified NPs, EDX measurements were performed. In Fig. 8, an EDX analysis of an agglomerate of APTES-perfluorooctanoic acid-modified zirconia nanoparticles deposited on an aluminum substrate is depicted. The detected elements (aluminum, zirconium, silicon and fluorine) are represented in different color images. Firstly, from aluminum and zirconium measurements the zirconia NP agglomerate (colored in pink) and the aluminum substrate (colored in purple) can clearly be distinguished. Secondly, the elements silicon and fluorine as components of perfluorooctanoic acid were analyzed, which proves the expected successful modification of the zirconia agglomerate by the predominant presence of these elements on the NP agglomerate.

We used the modified zirconia NPs to demonstrate the adjustment of the particle properties by the example of their hydrophobicity. To this end, coatings of NPs modified with different carboxylic acids with hydrophilic (by modification with adipic acid) to highly hydrophobic properties (by modification with perfluorooctanoic acid) were prepared on glass substrates by simple drop casting. To illustrate the effect of the NPs, *i.e.* the properties of the NP-based coatings, the contact angles of water on the pristine glass substrate and on the glass substrate coated with NP films of different APTES-CA-modified zirconia NPs are shown in Fig. 9.

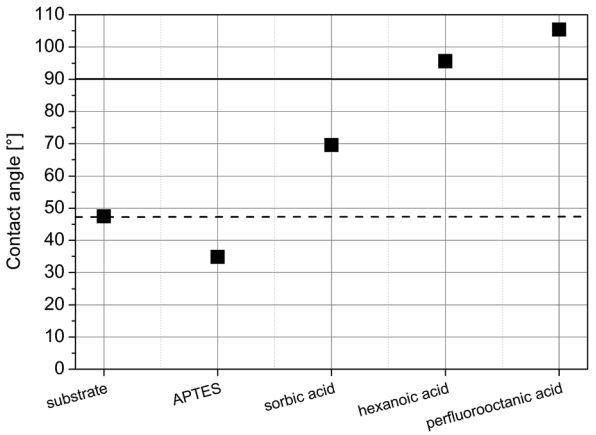

Fig. 9 Calculated contact angles of drop-cast films of zirconia NPs after two-step modification with different carboxylic acids in comparison to the pure glass substrate.

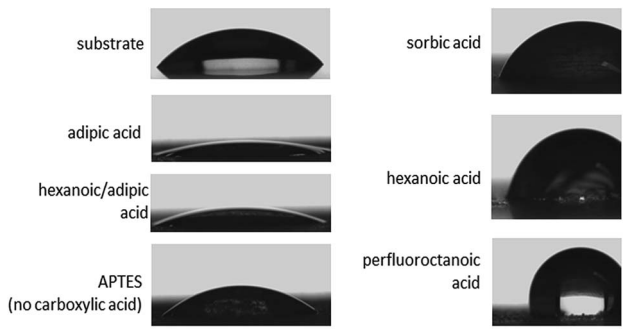

Fig. 10 Images of contact angle measurements of modified zirconia particles in the two step approach with different carboxylic acids.

For the pure glass substrate a contact angle of around 47° was measured with distilled water as liquid. The application of zirconia NPs after the first modification step with APTES leads to lower contact angles (35°) and, thus, to more hydrophilic properties of the particles in comparison to the glass substrate. After the second modification step – the coupling of the carboxylic acids – substantially higher contact angles from 70 to 105° were measured, depending on the used acid.

The contact angles for the NPs modified with adipic acid in the second step (as well as with a mixture of hexanoic and adipic acid) were too low to be reliably measured. The determined contact angles correspond to the wetting behaviour of the alkane chains of the coupled acids. The NPs modified with polar groups like adipic acid show highly hydrophilic properties, whereas the particles modified with less polar alkane chains show hydrophobicity in the order of the polarity of these groups. As example, the NPs modified with the moderately polar sorbic acid deliver a smaller contact angle than those modified with the non-polar hexanoic acid or the highly non-polar perfluorooctanoic acid. To further demonstrate the differences caused by the modification treatment, images of the developed water droplets on the prepared coatings are presented in Fig. 10.

The contact angle on a film consisting of NPs modified with both adipic and hexanoic acid in a molar ratio of 1 : 1 is only slightly higher than for modification with the pure adipic acid. This can be explained as an effect of the polar carboxyl groups (as mentioned above), which superimposes the weaker effect of the non-polar groups.

Conclusion

In this contribution, we presented a two-step modification strategy applicable to different nanoparticle systems to adjust and tailor the chemistry of the particle surface for different applications. The covalent binding of a first modifying agent (APTES) to commercial (Al_2O_3) as well as self-synthesized metal oxide nanoparticles (ZrO_2) with different sizes (100 nm for Al_2O_3 and 3 nm for ZrO_2) shows the broad applicability of the strategy to a variety of NP systems. As the second step, a straightforward organic coupling reaction was performed to further couple a number of different carboxylic acids to the nanoparticle surface. Whilst previous approaches relied on a complete change of the utilized ligands to realize different NP properties, in the presented approach only the carboxylic acid in the second coupling step has to be varied, with no need to adjust and optimize reaction conditions or further reagents. Each tested carboxylic acid was found to be firmly bound to the NP surface. To demonstrate the changes in chemical properties of the NPs, the contact angles of water on films of modified zirconia NPs were measured, proving that the hydrophobicity could be widely adjusted from highly hydrophilic to highly hydrophobic. Furthermore, the broad spectrum of available carboxylic acids that potentially can be coupled enables a further tailoring of the chemistry of the particle surface, in particular by the

introduction of further reactive groups in multifunctional carboxylic acids. Since such chemical groups can be used to greatly optimize the interaction between the nanoparticles and their vicinity, the proposed strategy offers high promise towards nanocomposites with enhanced properties due to its versatility and experimental simplicity.

Acknowledgements

We gratefully acknowledge financial support by the German Research Foundation (DFG, grants GA 1492/7-1 and KW 9/16-1).

References

1 S. Kango, S. Kalia, A. Celli, J. Njuguna, Y. Habibi and R. Kumar, *Prog. Polym. Sci.*, 2013, **38**, 1232–1261.
2 F. Hussain, M. Hojjati, M. Okamoto and R. E. Gorga, *J. Compos. Mater.*, 2006, **40**, 1511–1575.
3 S. Li, M. M. Lin, M. S. Toprak, D. K. Kim and M. Muhammed, *Nano Rev.*, 2010, **1**, 5214.
4 B. Wetzel, P. Rosso, F. Haupert and K. Friedrich, *Eng. Fract. Mech.*, 2006, **73**, 2375–2398.
5 R. Medina, F. Haupert and A. Schlarb, *J. Mater. Sci.*, 2008, **43**, 3245–3252.
6 J. H. Yu and G. Cennini, *Microelectron. J.*, 2014, **45**, 1829–1833.
7 H. J. Ahn, Y. J. Eoh, S. D. Park and E. S. Kim, *Thermochim. Acta*, 2014, **590**, 138–144.
8 W. Zhou, S. Qi, C. Tu, H. Zhao, C. Wang and J. Kou, *J. Appl. Polym. Sci.*, 2007, **104**, 1312–1318.
9 X. Liu, X. Liu, J. Wang, C. Liao, X. Xiao, S. Guo, C. Jiang, Z. Fan, T. Wang, X. Chen, W. Lu, W. Hu and L. Liao, *Adv. Mater.*, 2014, **26**, 7399–7404.
10 S. H. Stelzig, M. Klapper and K. Müllen, *Adv. Mater.*, 2008, **20**, 929–932.
11 Y. Wang, D. Zhang, L. Shi, L. Li and J. Zhang, *Mater. Chem. Phys.*, 2008, **110**, 463–470.
12 T. Cheema, A. Lichtner, C. Weichert, M. Böl and G. Garnweitner, *J. Mater. Sci.*, 2012, **47**, 2665–2674.
13 H. Lin, L. Li, J. Ren, Z. Cai, L. Qiu, Z. Yang and H. Peng, *Sci. Rep.*, 2013, **3**, 1353.
14 R. Gerson and T. C. Marshall, *J. Appl. Phys.*, 1959, **30**, 1650–1653.
15 T. A. Cheema and G. Garnweitner, *CrystEngComm*, 2014, **16**, 3366–3375.
16 G. N. Howatt, R. G. Breckenridge and J. M. Brownlow, *J. Am. Ceram. Soc.*, 1947, **30**, 237–242.
17 O. Masala and R. Seshadri, *Annu. Rev. Mater. Res.*, 2004, **34**, 41–81.
18 C. B. Ng, L. S. Schadler and R. W. Siegel, *Nanostruct. Mater.*, 1999, **12**, 507–510.
19 T. Hanemann and D. V. Szabó, *Materials*, 2010, **3**, 3468–3517.
20 R. Mueller, L. Mädler and S. E. Pratsinis, *Chem. Eng. Sci.*, 2003, **58**, 1969–1976.
21 G. Garnweitner, L. M. Goldenberg, O. V. Sakhno, M. Antonietti, M. Niederberger and J. Stumpe, *Small*, 2007, **3**, 1626–1632.
22 G. Garnweitner, in *Nanomaterials for the Life Sciences: Nanostructured Oxides*, ed. C. Kumar, Wiley-VCH, Weinheim, Germany, 2009, vol. 2.
23 T. Ninjbadgar, G. Garnweitner, A. Börger, L. M. Goldenberg, O. V. Sakhno and J. Stumpe, *Adv. Funct. Mater.*, 2009, **19**, 1819–1825.
24 Y. Wang, S. Zhang and X. Wu, *Nanotechnology*, 2004, **15**, 1162–1165.
25 Y. w. Jun, J. s. Choi and J. Cheon, *Angew. Chem.*, 2006, **45**, 3414–3439.
26 J. Lee, S. Zhang and S. Sun, *Chem. Mater.*, 2013, **25**, 1293–1304.
27 M. Kobayashi, R. Matsuno, H. Otsuka and A. Takahara, *Sci. Technol. Adv. Mater.*, 2006, **7**, 617–628.
28 Q. Wang, S. Ge and D. Zhang, *Wear*, 2005, **259**, 952–957.
29 Y. Wang, S. Lim, J. L. Luo and Z. H. Xu, *Wear*, 2006, **260**, 976–983.
30 E. Ritzhaupt-Kleissl, J. Boehm, J. Hausselt and T. Hanemann, *Mater. Sci. Eng., C*, 2006, **26**, 1067–1071.
31 M. Z. Rong, Q. L. Ji, M. Q. Zhang and K. Friedrich, *Eur. Polym. J.*, 2002, **38**, 1573–1582.
32 J. Pyun and K. Matyjaszewski, *Chem. Mater.*, 2001, **13**, 3436–3448.
33 K. Haraguchi, *Polym. J.*, 2011, **43**, 223–241.
34 D. Vollath and D. V. Szabó, *Adv. Eng. Mater.*, 2004, **6**, 117–127.
35 Y. Hu, S. Zhou and L. Wu, *Polymer*, 2009, **50**, 3609–3616.
36 G. Schmidt and M. M. Malwitz, *Curr. Opin. Colloid Interface Sci.*, 2003, **8**, 103–108.
37 A. Tok, F. Boey and X. Zhao, *J. Mater. Process. Technol.*, 2006, **178**, 270–273.
38 B. Schönstedt, N. Barth, G. Garnweitner, A. Mühlmeister and A. Kwade, *Langmuir*, 2011, **27**, 8396–8403.
39 L. T. Truong, Å. Larsen, B. Holme, S. Diplas, F. K. Hansen, J. Roots and S. Jørgensen, *Surf. Interface Anal.*, 2010, **42**, 1046–1049.
40 J. W. Krumpfer, T. Schuster, M. Klapper and K. Müllen, *Nano Today*, 2013, **8**, 417–438.
41 M. Bloemen, B. Sutens, W. Brullot, A. Gils, N. Geukens and T. Verbiest, *ChemPlusChem*, 2015, **80**, 50–53.
42 M. W. Daniels and L. F. Francis, *J. Colloid Interface Sci.*, 1998, **205**, 191–200.
43 R. B. Merrifield, *Endeavour*, 1965, **24**, 3–7.